Minimizing the Distortion of Steel Profiles by Controlled Cooling

Robert Pietzsch, Miroslaw Brzoza, Yalçin Kaymak, Eckehard Specht, Albrecht Bertram

Otto-von-Guericke-University, Magdeburg/Germany

A complex thermomechanical model is introduced for the simulation of the transient fields of temperature and stresses during the quenching of steel products. The material behaviour is an extension of the classical J_2-plasticity theory with the extension of temperature and phase fraction dependent yield criteria. The coupling effects, i.e., dissipation of mechanical energy, transformation induced plasticity (TRIP), and phase transformation enthalpy, are considered. The model is used for the determination of the optimal cooling or quenching for reducing the distortion in the long steel profiles. The simulation results are presented in order to investigate the effects of material properties, boundary conditions, profile size and geometry. In the simulations, L-, T- and U-profiles made of steel C45 and steel C80 are considered. It is demonstrated that with a higher cooling rate in the mass lumped regions of the profiles, the distortion can be reduced.

Keywords: steel quenching, TRIP, J_2-plasticity, thermo-elasto-plasticity, solid phase change, cooling of profiles, distortion minimisation.

Introduction

A heat treatment process is a common manufacturing process to produce steel profiles with reliable service properties. However, during the process, the residual stresses and distortion should be controlled to prevent crack initiation. Furthermore, controlling the microstructural evolution is important for achieving a specific hardness distribution.

The modelling of a heat treatment process is difficult because of the complicated couplings between different physical and mechanical processes. The thermal stresses in the profile are produced by large temperature gradients. The microstructural evolution significantly influences the stress field because solid-solid phase transitions are accompanied by density variation and transformation plasticity. On the other hand, the phase transition behaviour is affected by any stress/strain state existing in the volume. This is called stress induced transformation. During the heat treatment process, the internal stress field is continuously varied due to all these mechanisms. At any point in the profile, when the stress state exceeds the yield limit, or when transformation plasticity initiates for some temperatures, non-uniform or unsymmetric plastic deformations can occur. This causes a residual stress state at the end of the process which may be beneficial or detrimental.

The cooling of the steel profiles has been widely studied experimentally and analytically which are published in the literature. The distortions and residual stresses of railway profiles were measured in [1]. The effects of radiation and contact heat transfers as well as the frictional effects were described for railway profiles. The distortion of channel profiles was tested experimentally by the company Arbed and the results were presented in a research report in 1989. The distortion problem was extensively studied by European Union supported projects. The European Coal and Steel Company (ECSC) published the results in the internet site http://apollo.cordis.lu.

We assume that the temperature field and cooling conditions are the same along the profile. Hence, all the field variables will be the same along the profile as well. This assumption leads us to a two dimensional simulation which is sufficient to estimate the behaviour of the prismatic profile under such conditions with much fiever degrees of freedom. In addition, the dimensional reduction of the problem from three-dimension to two-dimension substantially simplifies not only the visualisation of the field variables but also the determination of optimal cooling strategy.

Basic Equations

The mathematical model of the heat treatment is described by a thermoelastoplastic theory which also covers the phase transformation effects. The temperature field has a great influence on the microstructure and mechanical properties. Hence the temperature field must be simulated accurately. The latent heat of phase transformation is considered as an additional heat source or heat sink. The microstructural evolution is obtained by using the isothermal time-temperature-transformation (TTT-) diagrams charts. The diffusion controlled phase transformations are computed according to the Johnson-Mehl-Avrami equation and the displacive phase transformation is calculated from the Koistinen-Marburger equation [2]. For the determination of stress/strain field, a constitutive relation is established, which depends on temperature and phase fraction. The total strain tensor is additively decomposed into several parts, as usual. The introduced model is applicable to 2D- and 3D-problems.

Temperature field. The microstructure and mechanical properties are strongly temperature dependent. Hence the temperature field must be determined correctly for an accurate simulation. The latent heat of the phase transformation has to be taken into account. The heat conduction is governed by the Fourier law, after which the heat flux vector is parallel to the temperature gradient,

$$\mathbf{q} = -k\nabla T \tag{1}$$

where k is the heat conduction coefficient, $\mathbf{q}$ is heat flux vector, and T is the temperature. The heat treatment process is a transient heat conduction problem where the tempera-

ture field is governed by equation (2) for an isotropic solid. The thermal balance, by considering heat fluxes and heat sources only, in an isotropic solid leads to:

$$\nabla \cdot (k\nabla T) + q_v = \rho c_p \frac{\partial T}{\partial t} \,, \tag{2}$$

where q_v is the heat source

$$q_v = \lim_{\Delta V \to 0} \frac{\Delta Q_h}{\Delta V} \,, \tag{3}$$

and ΔQ_h is the heat generated in unit time in the volume of the system considered, ρ is the density of the medium, and c_p is the specific heat capacity.

For the initial temperature distribution, uniformity is assumed

$$T\,(x, y, z, 0) = T_0 \,. \tag{4}$$

The heat is transferred from hot profiles to the ambient by convection and radiation

$$-k\frac{\partial T}{\partial n} = \alpha\,(T_w - T_\infty) + \varphi\varepsilon\sigma\left(T_w^4 - T_\infty^4\right), \tag{5}$$

where T_w is the temperature of the body surface, T_∞ is the ambient temperature, φ is the view factor, ε is the emissivity of the steel, and $\sigma = 5.67{\cdot}10^{-8}$ W/m^2/K^4 is the Stefan Bolzmann constant.

The classical Galerkin finite element method is used to solve the differential equation of the transient heat conduction problem. The temperature field can be approximated by the expression

$$T \cong \sum_{i=1}^{N} H_i T_i \,, \tag{6}$$

where H_i are shape functions, T_i are nodal temperatures, and N stands for the number of nodes. By substitution of the temperature in the weak form of equation (2), we get a system of equations

$$K_{ij}T_j + C_{ij}\dot{T}_j = F_i \,, \tag{7}$$

where

$$\begin{aligned} K_{ij} &= \int_V \nabla H_i k \nabla H_j dV + \int_S H_i \alpha' H_j dS, \\ C_{ij} &= \int_V H_i \rho c_p H_j dV, \\ F_i &= \int_V H_i q_v dV + \int_S H_i \alpha' T_\infty dS \end{aligned} \tag{8}$$

with

$$\alpha' = \alpha + \varphi\varepsilon\sigma\left(T_w^2 + T_\infty^2\right)(T_w + T_\infty). \tag{9}$$

Microstructural evolution. The microstructural evolution is computed by performing a coupled finite element analysis. The phase transformations are modelled by discretising the cooling curves into a succession of small isothermal steps and using the isothermal TTT diagrams. The transformed volume fractions are then calculated isothermally during each time step. Every phase transformation is assumed to occur within the respective temperature interval.

Prior to the decomposition of austenite into pearlite or bainite, an incubation period occurs. This period is determined according to the Scheil's additivity rule [3], i.e., it is assumed that the nucleation is finished as soon as the sum S is equal to unity, and then the transformation begins

$$S = \int_0^{t_I} \frac{dt}{\tau\,(T\,(t), \xi)} \cong \sum_{i=1}^{n} \frac{\Delta t}{\tau\,(T_i, \xi)} = 1 \,, \tag{10}$$

where Δt is the length of time step, $\tau\,(T_i, \xi)$ is the time required for the transforming the phase fraction ξ (e.g. $\xi = 0.01$) at the constant temperature T_i. After the nucleation, phase growth begins. For the growth calculations, the experimental kinetics of ferrite, pearlite or bainite transformations under isothermal conditions are governed by the Johnson-Mehl-Avrami equation [4]

$$\xi_i = \xi_a^s\left(1 - \exp\left(-a_i \cdot t^{b_i}\right)\right), \tag{11}$$

where ξ_i is the transformed phase fraction of the i$^{\text{th}}$ phase, ξ_a^s is the volume fraction of austenite at the beginning of the transformation, t is the time passed, a_i and b_i are temperature dependent constants of the i$^{\text{th}}$ phase, and these constants are calculated from TTT-diagrams [5]. In the case of a martensitic transformation, between temperatures T_{Ms} and T_{Mf}, the amount of martensite is calculated by using the law established by Koistinen and Marburger [2]. Martensitic transformation is completely governed by the instantaneous temperature

$$\xi_M = \xi_a^s\,(1 - \exp(-a(T_{Ms} - T)). \tag{12}$$

Stress/strain field. A temperature and phase fraction dependent constitutive relation is established for the stress-strain relation. The total stress is related to the total elastic strain by a constitutive law

$$\mathbf{T} = C^e\,(T, \Xi) \cdot \mathbf{E}^e \,. \tag{13}$$

In finite element calculations, the time derivative of Eq.(13) is used, which is called the rate form

$$\begin{aligned} \dot{\mathbf{T}} &= C^e \cdot \dot{\mathbf{E}}^e + \dot{C}^e \cdot \mathbf{E}^e \\ &= C^e \cdot \dot{\mathbf{E}}^e + \left(\frac{\partial C^e}{\partial T} \cdot \dot{T} + \frac{\partial C^e}{\partial \Xi} \cdot \dot{\Xi}\right) \cdot \mathbf{E}^e \end{aligned} \tag{14}$$

However, in order to use equation (14), one has to determine the elastic part of the total strain rate. The total strain rate is additively decomposed into several parts

$$\dot{\mathbf{E}} = \dot{\mathbf{E}}^{T,\Xi} + \dot{\mathbf{E}}^{p} + \dot{\mathbf{E}}^{TRIP} + \dot{\mathbf{E}}^{e}, \tag{15}$$

where $\dot{\mathbf{E}}^{T,\Xi}$ and $\dot{\mathbf{E}}^{e}$ are the reversible parts and $\mathbf{E}^{p}$ and $\dot{\mathbf{E}}^{TRIP}$ are the irreversible parts.

The thermal and phase transition related part $\dot{\mathbf{E}}^{T,\Xi}$, which is reversible, can be obtained from

$$\mathbf{E}^{T,\Xi} = \left(\sqrt[3]{\frac{\rho_R}{\rho}} - 1\right)\mathbf{I}, \tag{16}$$

where ρ_R and ρ are the reference and current mixture densities, respectively. For a mixture of N phases, the thermal and phase transition strain rate is given by

$$\dot{\mathbf{E}}^{T,\Xi} = \left(-\frac{1}{3}\sqrt[3]{\frac{\rho_R}{\left(\sum_{i=1}^{N}\xi_i\rho_i\right)^4}}\right)\sum_{i=1}^{N}\left(\xi_i\frac{\partial\rho_i}{\partial T}\dot{T} + \rho_i\dot{\xi}_i\right)\mathbf{I} \tag{17}$$

where ρ_i is the temperature dependent density of the i^{th} phase.

For the computation of the plastic strain rates, an extended classical J_2-plasticity theory is used. The extension is that the yield strength of the mixture depends on both the temperature and phase fractions as well as the total equivalent plastic strain. The details of the model can be found in [5, 6]. The yield strength of the i^{th} is given in [5] by the expression

$$\begin{aligned}\sigma_{yi} &= \sigma_{yi}\left(\varepsilon^{p}_{eff}, T\right)\\ &= \sigma_{yi0} + \Delta\sigma_{yi\infty}\left(1 - \exp\left(-\sigma_i' \cdot \ln\left(1 + \varepsilon^{p}_{eff}\right)\right)\right)\end{aligned} \tag{18}$$

where ε^{p}_{eff} is the total effective plastic strain defined in equation (21), σ_{yi0} is the initial yield strength, $\Delta\sigma_{yi\infty}$ is the maximum increase in the yield strength, and σ_i' is a parameter for the rate of this increase for the corresponding phase. The yield strength of the mixture is estimated by

$$\sigma_y\left(\varepsilon^{p}_{eff}, T, \Xi\right) = \sum_{i=1}^{N}\sigma_{yi}\xi_i\,. \tag{19}$$

Now, we can define the yield criterion function [7,8]

$$F\left(\mathbf{T}, \varepsilon^{p}_{eff}, T, \Xi\right) = \sigma_{eff}\left(\mathbf{T}\right) - \sigma_y\left(\varepsilon^{p}_{eff}, T, \Xi\right) \tag{20}$$

Here σ_{eff} and ε^{p}_{eff} represent the effective stress and the effective plastic strain, respectively,

$$\begin{aligned}\sigma_{eff}(T) &= \sqrt{\frac{3}{2}S\cdot S},\\ S &= T - \frac{1}{3}tr(T)\,\mathbf{I},\\ \varepsilon^{p}_{eff} &= \int_0^t \dot{\varepsilon}^{p}_{eff}d\tau,\\ \dot{\varepsilon}^{p}_{eff} &= \sqrt{\frac{2}{3}\dot{\mathbf{E}}^{p}\cdot\dot{\mathbf{E}}^{p}},\end{aligned} \tag{21}$$

where $\mathbf{T}$ is the stress tensor and $\mathbf{S}$ represents the deviatoric stress tensor.

Yielding occur if and only if

$$\begin{aligned}&F(\mathbf{T}, \varepsilon^{p}_{eff}, T, \Xi) = 0,\\ &\kappa = \frac{\partial F}{\partial \mathbf{T}}\cdot\dot{\mathbf{T}} + \frac{\partial F}{\partial T}\dot{T} + \frac{\partial F}{\partial \Xi}\cdot\dot{\Xi} > 0,\end{aligned} \tag{22}$$

the yield condition and loading conditions are both satisfied.

Since the stress state must remain on the yield surface during the yielding, we get the consistency condition

$$\begin{aligned}\dot{F} &= \frac{\partial F}{\partial \mathbf{T}}\cdot\dot{\mathbf{T}} + \frac{\partial F}{\partial \varepsilon^{p}_{eff}}\dot{\varepsilon}^{p}_{eff} + \frac{\partial F}{\partial T}\dot{T} + \frac{\partial F}{\partial \Xi}\cdot\dot{\Xi}\\ &= \kappa + \frac{\partial F}{\partial \varepsilon^{p}_{eff}}\dot{\varepsilon}^{p}_{eff} = 0\end{aligned} \tag{23}$$

where the partial derivatives have the following definitions

$$\begin{aligned}\frac{\partial F}{\partial \mathbf{T}} &= \frac{d\sigma_{eff}}{d\mathbf{T}} = \sqrt{\frac{3}{2}}\frac{\mathbf{S}}{\|\mathbf{S}\|} = \sqrt{\frac{3}{2}}\mathbf{N},\\ \frac{\partial F}{\partial \varepsilon^{p}_{eff}} &= -\frac{\partial \sigma_y}{\partial \varepsilon^{p}_{eff}} = -\zeta,\\ \frac{\partial F}{\partial T} &= -\frac{\partial \sigma_y}{\partial T},\\ \frac{\partial F}{\partial \Xi} &= -\frac{\partial \sigma_y}{\partial \Xi}.\end{aligned} \tag{24}$$

If we insert equation (24) into equation (23), we get

$$\dot{F} = \dot{\sigma}_{eff} - \zeta\dot{\varepsilon}^{p}_{eff} - \frac{\partial \sigma_y}{\partial T}\dot{T} - \frac{\partial \sigma_y}{\partial \Xi}\cdot\dot{\Xi} = 0 \tag{25}$$

If the loading $\left(\dot{\mathbf{T}}, \dot{T}, \dot{\Xi}\right)$ is given, then the effective plastic strain can be obtained from equation (25)

$$\dot{\varepsilon}^{p}_{eff} = \frac{1}{\zeta}\left(\dot{\sigma}_{eff} - \frac{\partial \sigma_y}{\partial T}\dot{T} - \frac{\partial \sigma_y}{\partial \Xi}\cdot\dot{\Xi}\right) = \frac{\kappa}{\zeta} \tag{26}$$

An associative flow rule is assumed

$$\dot{\mathbf{E}}^{p} = \dot{\eta}\frac{\partial F}{\partial \mathbf{T}} = \dot{\eta}\sqrt{\frac{3}{2}}\mathbf{N} \tag{27}$$

If we insert equation (27) into the effective plastic strain rate expression given in equation (21), we get

$$\begin{aligned}\dot{\varepsilon}^{p}_{eff} &= \sqrt{\frac{2}{3}\left(\dot{\eta}\frac{\partial F}{\partial \mathbf{T}}\right)\cdot\left(\dot{\eta}\frac{\partial F}{\partial \mathbf{T}}\right)}\\ &= \sqrt{\frac{2}{3}\dot{\eta}^2\frac{3}{2}\mathbf{N}\cdot\mathbf{N}} = \dot{\eta}\end{aligned} \tag{28}$$

The TRIP strain rate is determined by the expression after Leblond [9]

$$\dot{\mathbf{E}}^{TRIP} = -\frac{3}{2}\Lambda \ln(\xi)\,\dot{\xi}\,\mathbf{S} \tag{29}$$

The term Λ in equation (29) is called as the Greenwood-Johnson factor [10] and it has the following meaning

$$\Lambda = \frac{5}{6}\frac{\rho_A - \rho_P}{\sigma_{yA}\cdot\rho_A} \tag{30}$$

Given $\left(\dot{\mathbf{E}}, \dot{\mathbf{E}}^{T,\Xi}, \dot{\mathbf{E}}^{TRIP}\right)$, we can compute the effective plastic strain rate by using equations (21-30)

$$\dot{\varepsilon}^{p}_{eff} = \frac{\sqrt{\frac{3}{2}}\mathbf{N}\cdot C^{e}\cdot\left(\dot{\mathbf{E}} - \dot{\mathbf{E}}^{T,\Xi} - \dot{\mathbf{E}}^{TRIP}\right) + \sqrt{\frac{3}{2}}\cdot\mathbf{N}\cdot\mathbf{T} - \frac{\partial\sigma_y}{\partial T}\dot{T} - \frac{\partial\sigma_y}{\partial\Xi}\cdot\dot{\Xi}}{\frac{3}{2}\mathbf{N}\cdot C^{e}\cdot\mathbf{N} + \zeta} \tag{31}$$

with

$$\mathbf{T}' = \dot{C}^{e}\cdot\mathbf{E}^{e} = \left(\frac{\partial C^{e}}{\partial T}\dot{T} + \frac{\partial C^{e}}{\partial\Xi}\cdot\dot{\Xi}\right)\cdot\mathbf{E}^{e} \tag{32}$$

and the stress rate is given by

$$\begin{aligned}\dot{\mathbf{T}} =& C^{ep}\left[\dot{\mathbf{E}} - \dot{\mathbf{E}}^{T,\Xi} - \dot{\mathbf{E}}^{TRIP}\right] \\ &+ K_L\left\{\frac{2}{3}\sigma_{eff}\left(\frac{\partial\sigma_y}{\partial T}\dot{T} + \frac{\partial\sigma_y}{\partial\Xi}\cdot\dot{\Xi}\right) - \mathbf{S}\cdot\mathbf{T}'\right\}\mathbf{S} + \mathbf{T}'\end{aligned} \tag{33}$$

with

$$\begin{aligned}K_L &= \frac{3G}{\left(\sigma_{eff}\right)^2\left(2G + \frac{2}{3}\zeta\right)}, \\ C^{ep} &= C^{e} - 2GK_L(\mathbf{S}\otimes\mathbf{S}).\end{aligned} \tag{34}$$

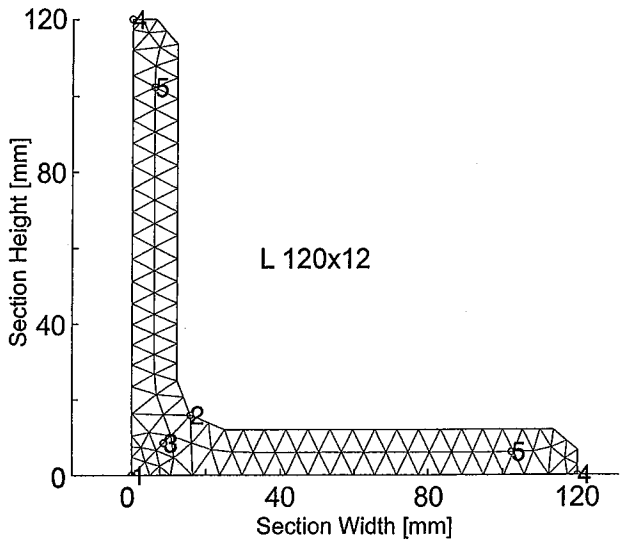

Figure 1. Investigated points and FE-mesh of the cross-section of an L-profile.

The mathematical model is used to estimate the hardness of steel 100Cr6. The simulation results agree with the experimental results given in the AiF-report [11].

Simulation Results

The mathematical model introduced above is used for the determination of the optimal cooling strategy for reducing the distortion and residual stresses in the long steel profiles. The effects of boundary conditions, profile sizes and profile geometries are investigated by using L-, T- and U-profiles. As a profile material, steel C45 and C80, for which the material properties are given in [4,5], are considered in the simulations. These two steel have different carbon content. Pearlitic steel C45 is an under-eutectoid steel. However, ferritic/pearlitic steel C80 is a eutectoid steel.

Cooling of L-profiles. In order to understand the mechanism and the behaviour of the cooling of the L-profiles, many simulations are carried out by varying the section size, material properties and heat transfer coefficients. The geometric details are taken according to DIN1028. The material effect is investigated by using two different materials, C45 and C80. To interpret the field variables like temperature, phase fractions, stress/strain components, etc., five sampling points which are shown in **figure 1** are chosen.

L120x12 profiles are cooled according to cooling strategy 1 (see figure 5) with a heat transfer coefficient α_1 = 20W/m^2/K. Time variations of field variables are shown in **figure 2**. The first row shows the temperature history. The fastest cooling occurs at point 1 and the slowest cooling occurs at point 3. Therefore, the phase transformation first starts at point 1 as given in the second row. The phase transition starts approximately at 730°C and finishes around 670°C. During the phase transformations, the axial stress component frequently changes sign and reaches a maximum at the end of the phase transformation. Similar to the axial stress, the axial TRIP strain component also fluctuates during the phase transformation.

The definition of distortion is given in [5]. Unlike the deflection, which varies with the length of the profile, the distortion is defined as a measure for the curvature, which is independent of the profile length. The distortion histories are shown for C45 and C80 steels in **figure 3**. In general, the curve can be considered as composed of three parts. The first part contains the elastic range. In the second part, the plastic deformations start due to fast cooling and phase transformation. This part can be further divided into two subparts for ferritic steel, but these are not of special interest here. In the third part, most of the elastic distortions fade away slowly. Each of these three parts, which are indicated in Fig. 3, contains a phase transformation induced distortion turning point. Indeed, the finial residual distortion is mainly due to the transformation induced plasticity (TRIP).

The spatial distribution of the axial component of the stress tensor at the end of the cooling is shown in **figure 4**. In the contour plot, the bold line, which is called zero-line, represents the zero stress level. Therefore, it is a limit between the regions of tension and compression. The same

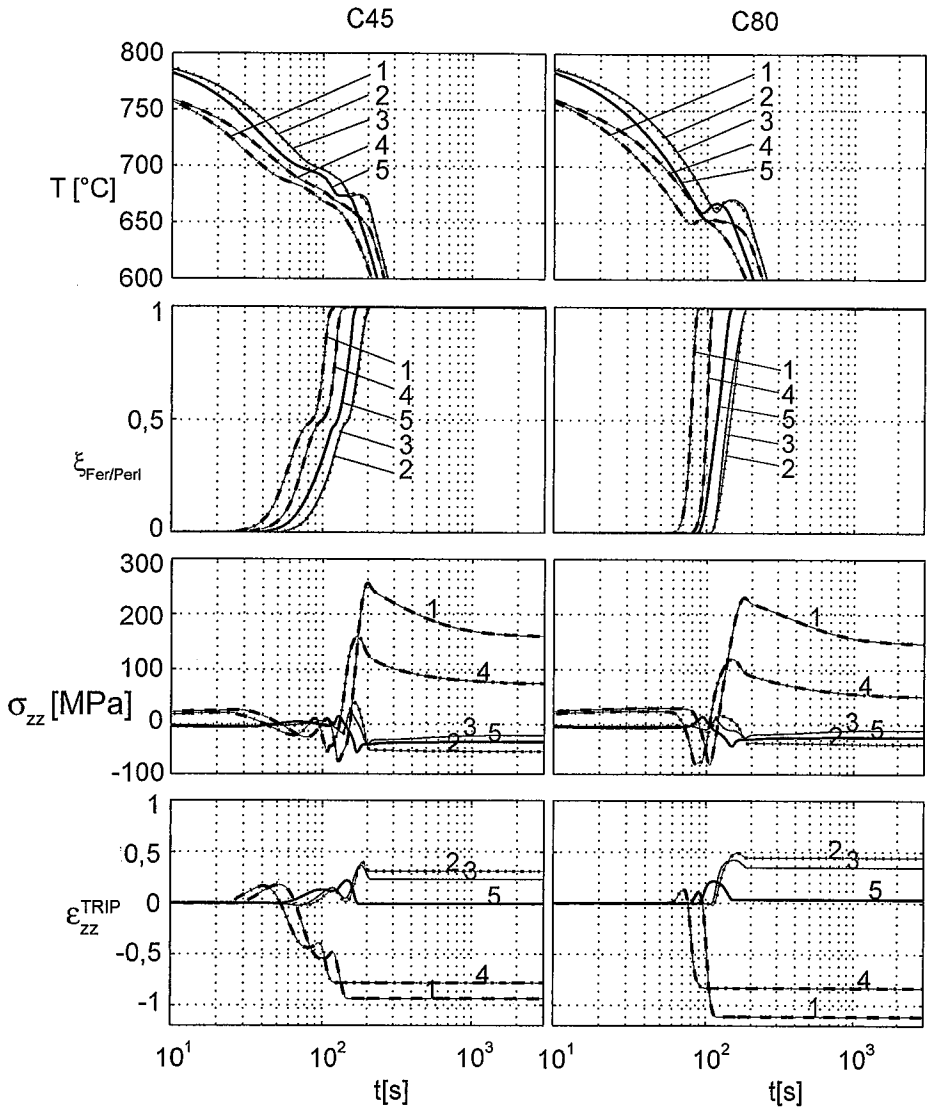

Figure 2. Time variations of the field variables at the respective points of the L-profile (cf. figure 1).

distribution or topology can be visualised better by the 3D plot in the figure on the right side.

Influence of Cooling. For the cooling of L-profiles, four different cooling strategies are considered, which are practically applicable with different cooling intensities (see **figure 5**). The heat transfer coefficient for the normally cooled regions is taken as $\alpha_0 = 10 W/m^2/K$ which may be a typical value for free convection. For the radiation cooling, the heat emissivity is $\varepsilon = 0.7$. The main principle of the cooling strategies is to increase the cooling at the mass lumped part as shown in figure 5. The heat transfer coefficient for the regions with forced cooling depends on α_1 which can be adjusted for example by a row of nozzles with air flow.

An increase in the heat transfer coefficient α_1 has great influence on the final distortion. Some simulations have been carried out with L120x12 section and C80 material. The simulation result can be seen in **figure 6**. When using the cooling strategy 1, i.e. when the L-profile is cooled from outer side with a heat transfer

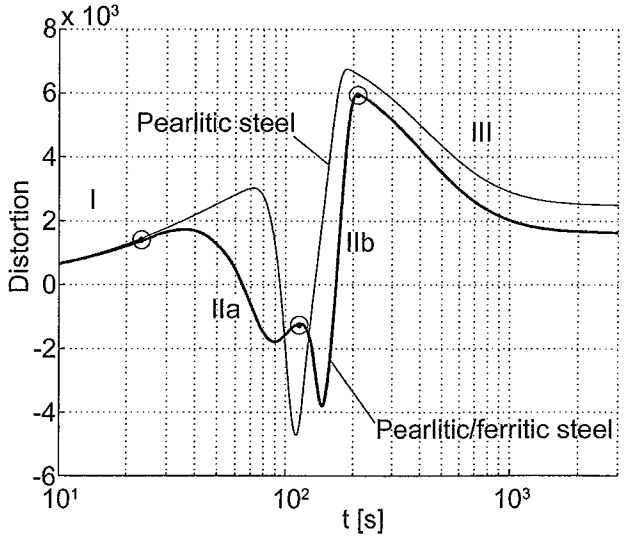

Figure 3. Distortion history for an L-profile.

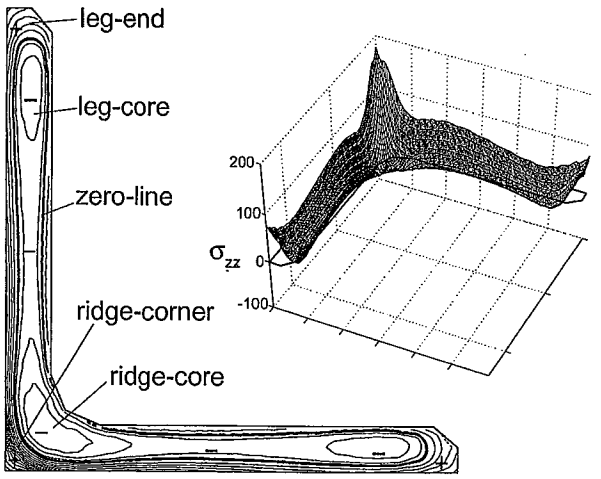

Figure 4. Contour line and 3D representation of the residual axial stress (σ_{zz} [MPa]).

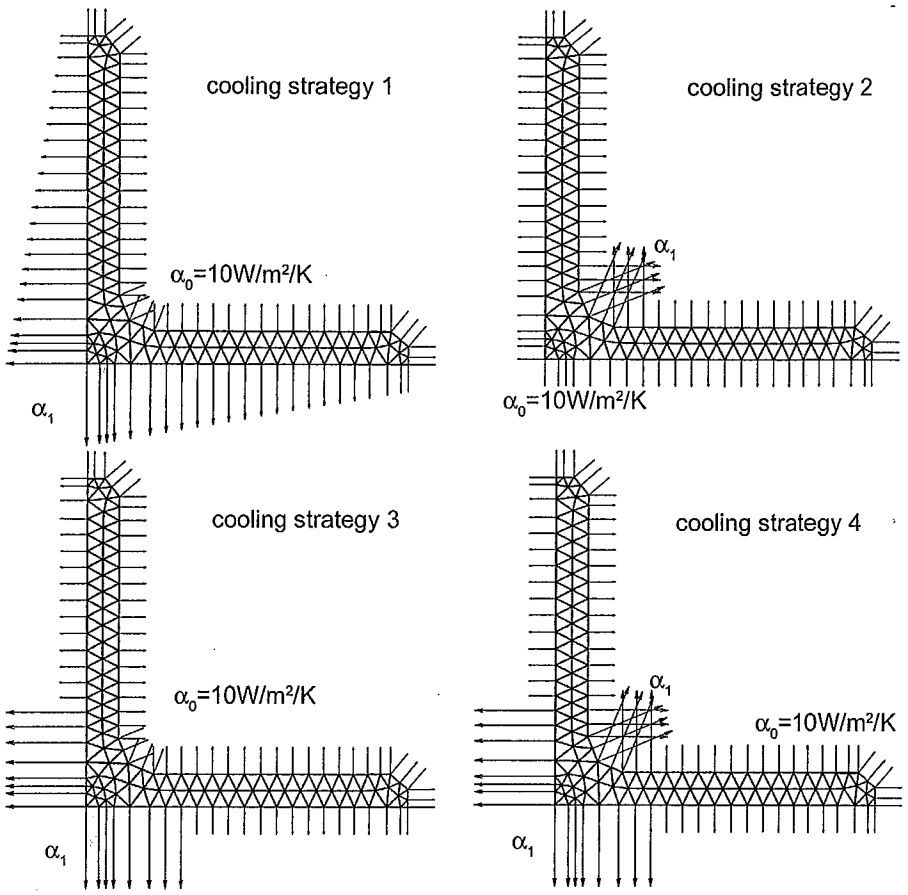

Figure 5. Schematic representation of different cooling strategies.

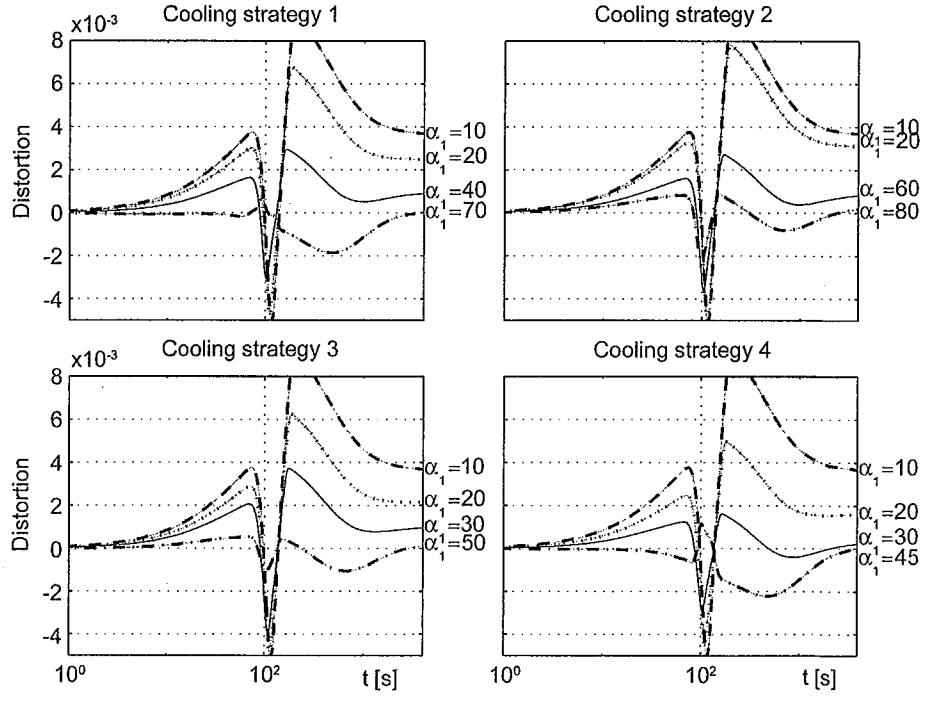

Figure 6. Distortion history for L120x12 profile of C80 steel for varying cooling conditions (cf. figure 5).

coefficient α_1 = 70W/m²/K, the distortion of the profile can almost be eliminated. If the heat transfer coefficient is α_1 > 70W/m²/K, then the direction of the distortion is reversed, which is not shown here. In strategy 2, the L-profile is cooled from the inner side. This time, the distortion is greatly reduced when the heat transfer coefficient is α_1 = 80W/m²/K. As an alternative cooling strategy, the mass lumped part can be locally cooled from outer side which is described in cooling strategy 3. For this cooling, if the heat transfer coefficient is chosen α_1 = 50W/m²/K, there is almost no distortion. Finally, in the strategy 4, the corner is cooled locally from both inner and outer sides. Most of the distortion is avoided for the heat transfer coefficient α_1 = 45W/m²/K. There are infinitely many cooling strategies, but here only four of them are described. Hence it is possible to reduce the distortion by adjusting the cooling. It is not important how the mass lumped regions are cooled as long as the cooling rate is increased at these regions.

The L-profiles, which are cooled according to the different cooling strategies described above are analysed for residual stresses. In **figure 7**, the variations of residual stress distributions through the section cut A-A are shown. Depending on the cooling strategy, the residual stress distributions vary. Before choosing a cooling strategy, the residual stress distribution should also be considered.

Influence of the Section Size. Three different size L-profiles, L60x6, L120x12 and L180x18, are analysed to investigate the size effect. The distortion histories are compared in **figure 8**. It can be stated that the distortion is inversely proportional to the

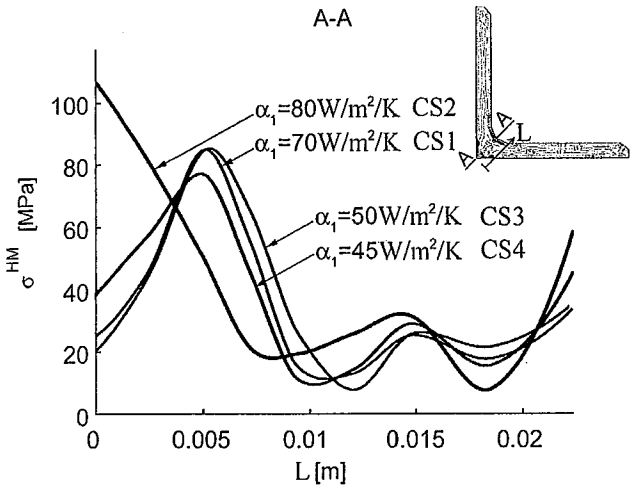

Figure 7. Variation of the effective residual stress with different cooling strategies (cf. figure 5).

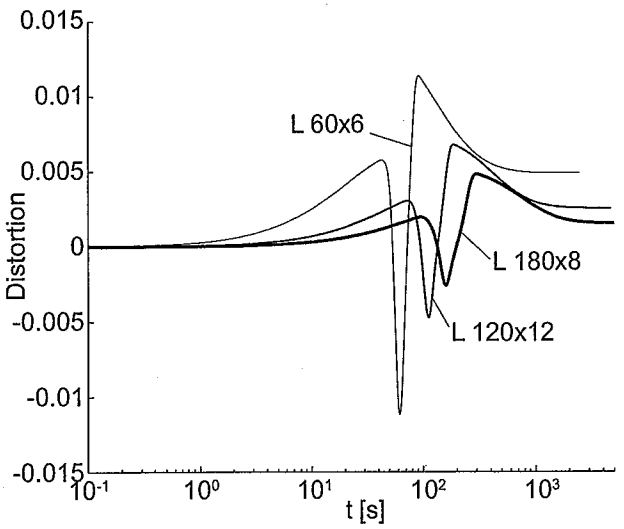

Figure 8. Influence of the cross-section size on the distortion.

section size, since the bigger sections have a much higher moment of resistance. When the sections get bigger, the thermal induced moments increase as well. However, the increase in the thermal induced moment is not as much as the increase in moment of resistance.

The section size also affects the residual stress distributions. The different size L-profiles are cooled according to strategy 1 with a transfer coefficient of $\alpha_1 = 20 W/m^2/K$. The variation of equivalent residual stress through a section cut A-A is plotted as a function of dimensionless length in **figure 9**. It is obvious that if the section size increases, the peak stress in the corner is reduced and moves to the inside of the section.

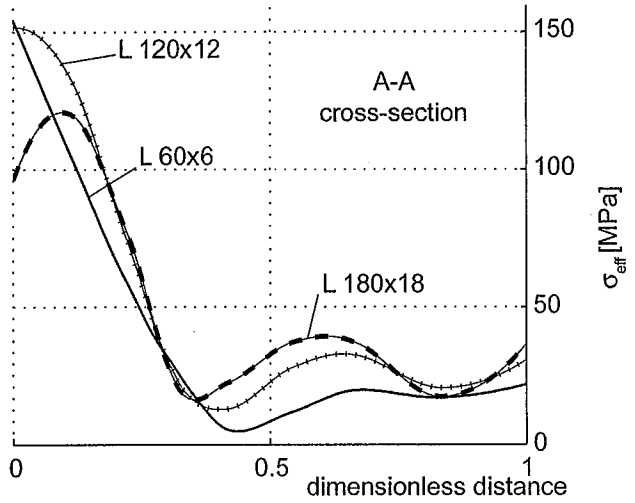

Figure 9. Residual stress distribution for L-profiles of different size.

Influence of the Shape. T- and U-profiles are considered to investigate the shape effect. T-profile dimensions are taken according to DIN 1024, and U-profile geometry details according to DIN 1026 standards. First, the T-profile is analysed. Two different cooling strategies are considered. The cooling strategy 1 (**figure 10**) is to increase the cooling rate in the mass lumped region from the iner side of the profile. Whereas the strategy 2 (**figure 11**) cools from the bottom part for the same purpose by using the equation, $\alpha(x) = \alpha_0 + \alpha_1 \exp(-B\,x^2)$. In this equation, the parameter B is a shape parameter.

The distortion of the profile is almost avoided by using the cooling strategy 1 with a heat transfer coefficient of $\alpha_1 = 45 W/m^2/K$. In figure 10, it is observed that, when the heat transfer coefficient increases, the maximum distortion decreases. Also, notice that for $\alpha_1 = 60 W/m^2/K$, the distortion is in the reverse direction.

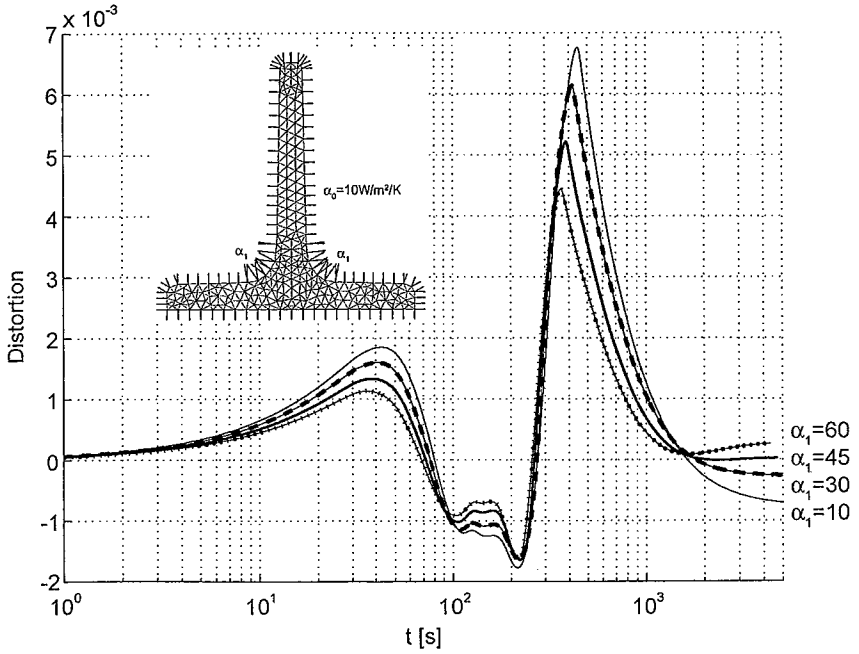

Figure 10. Distortion histories for T120 profile of C45 steel for cooling strategy 1.

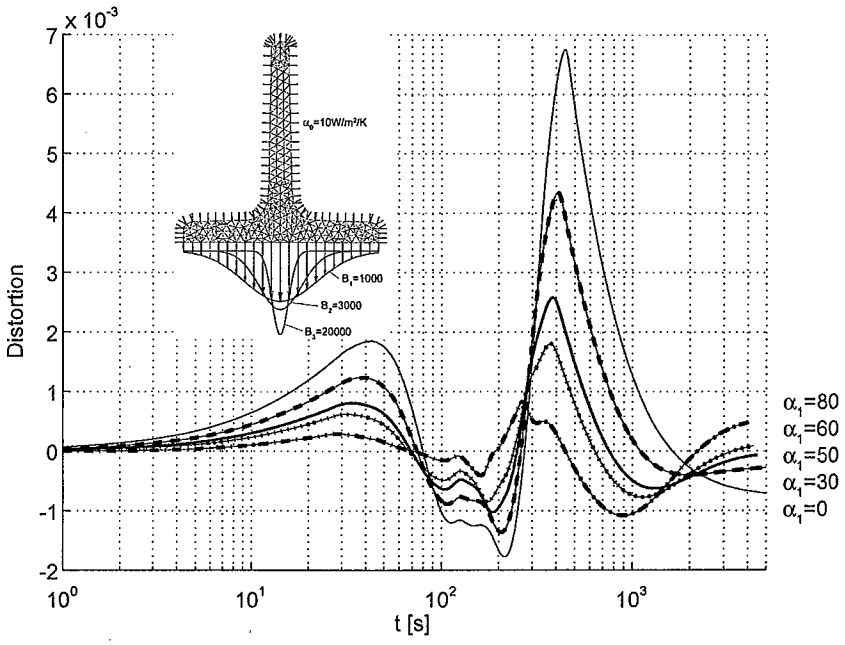

Figure 11. Distortion histories for T120 profile of C45 steel for cooling strategy 2.

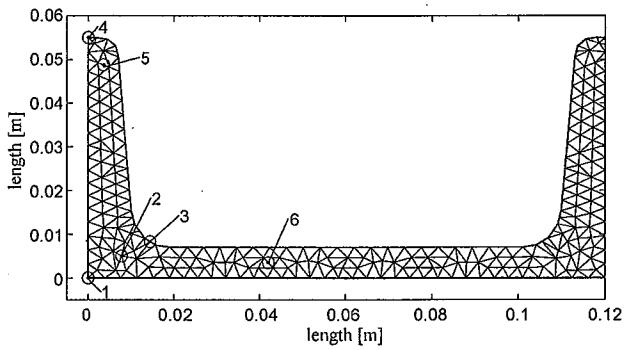

Figure 12. Regarded points and FE-mesh of the U-profile cross-section.

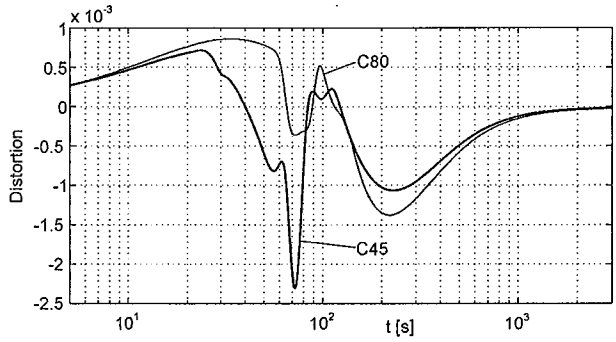

Figure 13. Distortion history of the U-profile.

The distortion is reduced by cooling the mass lumped part from the outer side. For this cooling strategy the shape parameter B has a great influence on the results. When the distribution is wide with a shape parameter B = 1000, the profile needs to be cooled with a heat transfer coefficient of α_1 = 55W/m^2/K. On the other hand, when the distribution is narrow (B=20000), a much higher heat transfer coefficient α_1 = 130W/m^2/K is required because the area for high heat transfer is reduced. The distortion can be avoided by both strategies because it does not matter whether the cooling is from the outer or from the inner side of the profile. All practical application strategies base on increasing the cooling at mass lumped regions as compared to the thinner parts.

The U-profiles were produced by hot rolling process. The cooling of a U-profile with a section size 120mm x 55mm from 800°C is simulated. The convection and radiation cooling effects are considered. The radiation emissivity is assumed to be ε = 0.7. In order to observe the variation of the field variables, six points are considered which are shown in **figure 12.**

The distortion histories are shown in **figure 13** for two different types of steels, C80 and C45. A uniform cooling is considered with a heat transfer coefficient of 10W/m^2/K. Since there is no distortion at the end of the uniform cooling, it is not necessary to use any other strategy. The difference in distortion histories is because of the varying material properties. C45 is a pearlitic type of steel. However, C80 is a pearlitic/ferritic type of steel. The equivalent stresses given in [5] have a maximum value of 35MPa. This stress level is much smaller as compared to those in T- and L-profiles.

Conclusions

A mathematical model is developed to simulate the transient temperature field, phase fractions, stress/strain fields, and distortion of long steel profiles. Many simulations are carried out to investigate the effect of varying shape, size, cooling strategy, and material properties. It is always possible to reduce the distortion of the profile by increasing the cooling at mass lumped regions. Some of the facts that can be concluded form the simulation results are listed as follows:

- Profiles with smaller section size show higher distortion than those with bigger section size. This fact has already been known in practice.
- U-profiles have no distortion after the cooling. This fact has been verified once more by the simulation results.
- Sections with pearlitic steel has higher distortion during the phase transformation period than those with ferritic/pearlitic steel.
- The distortion is mainly due to the TRIP strains which are related to the phase transformation phenomena.
- It is always possible to reduce the distortion by increasing the cooling rate in mass lumped regions. It is not important which cooling strategy is used to increase the cooling

rate in those regions as long as only the distortion is considered.

Acknowledgement

This project was founded by German Research Foundation (DFG) within the "Graduiertenkolleg 828, Micro-Macro-Interactions in Structured Media and Particle Systems". Thanks to DFG for the promotion of the work.

(A2004106; received on 20 July 2004, in final form on 5 November)

Contact:
Prof. Dr.-Ing. Eckehard Specht
Otto-von-Guericke Universität
FVST – ISUT, Postfach 4120
39016 Magdeburg / Germany

References

[1] E. Hinteregger: Eigenspannungen und Verformung in Schienen nach dem Walzen vor dem Richten, Dr-Ing. Thesis, Montanuniverstät Loeben, 1990.
[2] D.P. Koistinen, R.E. Marburger: Acta Metallica, 7 (1959), 59-60.
[3] E. Scheil: Archiv Eisenhüttenwesen, 12 (1935), 565-570.
[4] W.A. Johnson, P.A. Mehl: Trans AIMME 135 (1939), 416.
[5] R. Pietzsch: Simulation und Minimierung des Verzuges von Stahlprofilen bei der Abkühlung, Dr.-Ing. Thesis, Otto-von-Guericke-Universtät Magdeburg, 2000, Shaker-Verlag.
[6] H.P. Hougardy: Umwandlung und Gefüge unlegrerter Stähle, Verlag Stahleisen, Düsseldorf, 1990.
[7] A. Bertram: Int. J. Plasticity, 19 (2003), 2027-2050.
[8] S. Dachkovski; M. Böhm: Int. J. Plasticity, 20 (2004), 323-334.
[9] J.-B. Leblond, J. Devaux, J.C. Devaux: Int. J. Plasticity, 5 (1989), 551-572.
[10] G.W. Greenwood, R.H. Johnson: Proced. R.S. London , A283 (1965), 403-422.
[11] J. Ohland, O. Belkessam, Th. Lübben, U. Fritsching, P. Mayr, M. Brzoza, E. Specht: Härten von Werkstücken mit komplexer Geometrie und Minimierung des Verzuges durch flexible Gasabschreckung, Final Report of Research Project AiF 12012 B, 2002.

steel research international

Publishers:
Steel Institute VDEh
Max-Planck-Institut für Eisenforschung
Austrian Society for Metallurgy and Materials ASMET

Publishing company:
Verlag Stahleisen GmbH
Sohnstraße 65, D-40237 Düsseldorf

CONTENTS